Preprints.org

Article

Not peer-reviewed version

A Novel Red-Emitting NaYS2 Phosphor Under 1550 nm Excitation

Jiulong Wu *, Ying Tian *, Limin Wei , Ke Cai , Xixian Luo , Hong Wang *

Posted Date: 25 November 2023

doi: 10.20944/preprints202311.1596.v1

Keywords: NaYS2; red up-conversion luminescence; 1550 nm

Preprints.org is a free multidiscipline platform providing preprint service that is dedicated to making early versions of research outputs permanently available and citable. Preprints posted at Preprints.org appear in Web of Science, Crossref, Google Scholar, Scilit, Europe PMC.

Copyright: This is an open access article distributed under the Creative Commons Attribution License which permits unrestricted use, distribution, and reproduction in any medium, provided the original work is properly cited.

Preprints (www.preprints.org) | NOT PEER-REVIEWED | Posted: 25 November 2023 doi:10.20944/preprints202311.1596.v1

Disclaimer/Publisher's Note: The statements, opinions, and data contained in all publications are solely those of the individual author(s) and contributor(s) and not of MDPI and/or the editor(s). MDPI and/or the editor(s) disclaim responsibility for any injury to people or property resulting from any ideas, methods, instructions, or products referred to in the content.

Article

A Novel Red-Emitting $NaYS_2$ Phosphor under 1550 nm Excitation

Jiulong Wu, Ying Tian *, Limin Wei, Ke Cai, Xixian Luo and Hong Wang *

School of Science, Dalian Maritime University, Dalian 116026, China

* Correspondence: tianying@dlmu.edu.cn (Y.T.); wanghong@dlmu.edu.cn (H.W.)

Abstract: Up-conversion luminescence (UCL) materials are of great importance due to their unique optical properties. In particular, the red UCL, falling into the optical transmittance window of biological tissues, can realize deep tissue penetration depth and high-resolution bioimaging. In this work, effective red UCL is achieved in the ternary sulfide by the introduction of Tm^{3+} or Ho^{3+} ions into Er^{3+} doped $NaYS_2$ under 1550 nm excitation. The main emission peak is successfully tuned from green ($NaYS_2:Er^{3+}$) to highly efficient red luminescence ($NaYS_2:Er^{3+},Tm^{3+}$ and $NaYS_2:Er^{3+},Ho^{3+}$). The maximum red to green emission intensity ratio (I_R/I_G) increased by 31 and 80 times, respectively. The lifetime of $^4I_{9/2}(Er^{3+})$ level decreases significantly from 3432 μs ($NaYS_2:Er^{3+}$) down to 636 ($NaYS_2:Er^{3+},Tm^{3+}$) and 423 μs ($NaYS_2:Er^{3+},Ho^{3+}$), respectively. This is due to the altered energy transfer pathways, resulting in the population of $^4F_{9/2}(Er^{3+})$. The mechanisms of UCL and energy transfer processes are further supported by fluorescence decay dynamic measurements. The results show the realization of red-emissive UCL in the promising $NaYS_2$ matrix, representing a new type of red UCL phosphors.

Keywords: $NaYS_2$; red up-conversion luminescence; 1550 nm

1. Introduction

Lanthanide ions (Ln^{3+})-doped up-conversion luminescence (UCL) materials have attracted significant interests in the areas of display, sensing, anti-counterfeiting, bioimaging and diagnostics owing to their superior optical properties of sharp and tunable 4f → 4f emissions, resistance to photobleaching and no autofluorescence background [1–6]. However, the utilization of UCL material as a luminescence probe for bioimaging is currently restricted by the strong absorption of short-wavelength light (below 600 nm) by the tissues, resulting in limited efficacy [7]. Therefore, the development of red emissions in the "tissue transparent window" (600-1200 nm) is of great significance in achieving deep tissue penetration depth and high-resolution bioimaging [8–12]. For Ln^{3+}-doped UCL, it is known that a host crystal lattice with low symmetry is essential to relax the Laporte selection rule and significantly enhance f-f emissions [13]. Additionally, the ideal host material should possess low lattice phonon energy to minimize non-radiative multi-phonon relaxation, enhance electron population of excited states, and prolong the excited state lifetime [14,15]. Currently, research into Ln^{3+}-doped UCL materials has predominantly focused on fluoride hosts, particularly β-$NaYF_4$, which is renowned for its low phonon energy (418 cm^{-1}) and asymmetric hexagonal crystal structure [16–24]. However, the $NaYF_4$ is easy to deliquescence in humidity environment due to their poor chemical stability, which finally quench the UCL of Ln^{3+} [25]. Recently, Luo et al have found a new host of ternary rare earth sulfide with phonon energy of 279 cm^{-1}, which is even lower than that of β-$NaYF_4$ and have proven its high quantum yield of UCL under excitation of ~1550 nm [26,27]. However, both Er^{3+} single-doped and Yb^{3+}/Er^{3+} co-doped $NaYS_2$ samples exhibit strong green emission due to the long fluorescent lifetime of Er^{3+} at $^4I_{9/2}$ energy level which results in the favorable population of the green-emitting level ($^2H_{11/2}/^4S_{3/2}$). The red UCL has not been achieved in this promising ternary sulfide matrix material.

© 2023 by the author(s). Distributed under a Creative Commons CC BY license.

Preprints (www.preprints.org) | NOT PEER-REVIEWED | Posted: 25 November 2023 doi:10.20944/preprints202311.1596.v1

In this work, Tm^{3+} and Ho^{3+} ions are introduced into Er^{3+} doped $NaYS_2$ material to achieve pure and efficient red UCL under 1550 nm excitation. The results show that the I_R/I_G significantly promotes by 31 and 80 times, respectively. This is due to the newly generated energy transfer pathways after cooperating with Tm^{3+} and Ho^{3+} ions. The mechanisms of UCL and energy transfer processes are investigated in detail by steady-state fluorescence spectra and dynamics luminescence decay measurements.

2. Results and Discussions

The XRD patterns of $NaYS_2$:6%Er^{3+},0.5%Tm^{3+} and $NaYS_2$:6%Er^{3+},0.5%Ho^{3+} samples are shown in Figure 1a. As shown in the figure, all the peaks can be well indexed to trigonal crystal structure $NaYS_2$ with space group of $R\bar{3}m$ (PDF#46-1051). This indicates that the pure trigonal $NaYS_2$ are successfully synthesized for the $NaYS_2$:6%Er^{3+},0.5%Tm^{3+} and $NaYS_2$:6%Er^{3+},0.5%Ho^{3+} phosphors. The crystal structure of $NaYS_2$ belongs to the α-$NaFeO_2$-type structure. The [NaS_6] and [YS_6] octahedrons are arranged into alternating layers through edge sharing, which are perpendicular to the *c* axis of the crystal (Figure 1b) [28,29]. The SEM images (Figure 1c and d) show that the sample presents irregular shapes and are agglomerate, which may due to the high synthesis temperature.

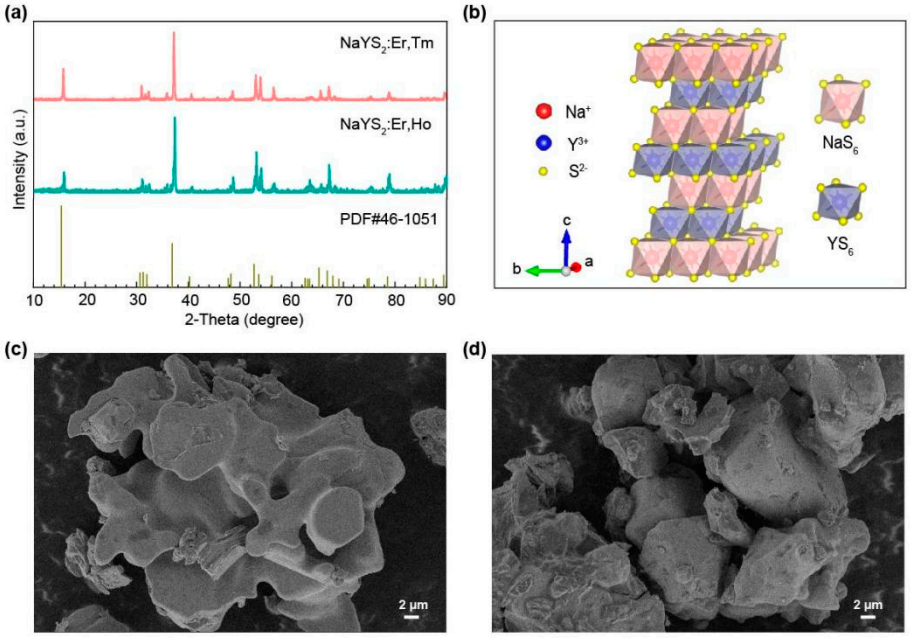

Figure 1. (a) XRD patterns of $NaYS_2$:6%Er^{3+},0.5%Tm^{3+} and $NaYS_2$:6%Er^{3+},0.5%Ho^{3+} samples along with a standard pattern of trigonal $NaYS_2$ (PDF#46-1051). (b) Crystal structural diagram of $NaYS_2$. (c) and (d) are SEM images of $NaYS_2$:Er^{3+} sample.

The optical properties of Er^{3+}/Tm^{3+} and Er^{3+}/Ho^{3+} co-doped $NaYS_2$ samples are investigated and presented in Figure 2. The reflection spectra of Er^{3+}/Tm^{3+} and Er^{3+}/Ho^{3+} co-doped $NaYS_2$ samples exhibit same reflection peaks at 365, 379, 405, 452, 489, 525, 555, 655, 799, 974, 1473 and 1537 nm, which correspond to the electronic transitions of Er^{3+} ions. It is clearly shown that in both samples, the absorption at 1550 nm is much stronger than that at 980 nm. This is due to the large absorption cross-section of Er^{3+} ion at $^4I_{13/2}$ energy level. The reflection peaks at 463, 686, 777, 1133 and 1207 nm correspond to the transitions of $^5I_8 \rightarrow {}^5F_2$, $^3H_6 \rightarrow {}^3F_2$, $^3H_6 \rightarrow {}^3H_4$, $^5I_8 \rightarrow {}^5I_6$ and $^3H_6 \rightarrow {}^3H_5$ of Ho^{3+} or Tm^{3+} ions, respectively.

Preprints (www.preprints.org) | NOT PEER-REVIEWED | Posted: 25 November 2023 doi:10.20944/preprints202311.1596.v1

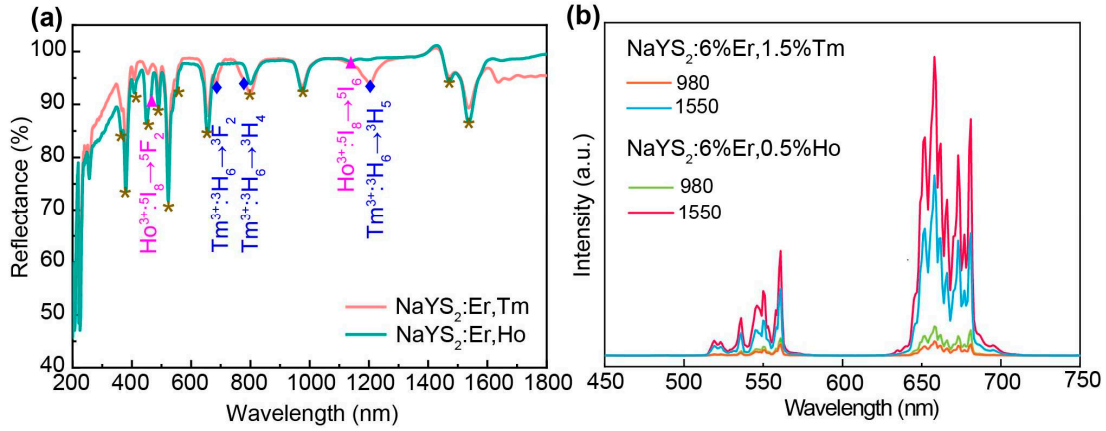

Figure 2. (a) Diffuse reflectance spectra of $NaYS_2$:6%Er^{3+},0.5%Ho^{3+} and $NaYS_2$:6%Er^{3+},1.5%Tm^{3+}. (b) Up-conversion luminescence (UCL) spectra of $NaYS_2$:6%Er^{3+},1.5%Tm^{3+} and $NaYS_2$:6%Er^{3+},0.5%Ho^{3+} at 980 and 1550 nm excitations, respectively, by utilizing the same laser power of 96 mW.

As shown in Figure 2b, the $NaYS_2$:6%Er^{3+},0.5%Ho^{3+} and $NaYS_2$:6%Er^{3+},1.5%Tm^{3+} samples exhibit relatively weak green emissions at 515 ~ 565 nm and intense red emission bands at 640 ~ 680 nm, which are assigned to the $^2H_{11/2}/^4S_{3/2} \rightarrow {}^4I_{15/2}$ and $^4F_{9/2} \rightarrow {}^4I_{15/2}$ transitions of Er^{3+} ions, respectively. The UCL of $NaYS_2$:6%Er^{3+},1.5%Tm^{3+} and $NaYS_2$:6%Er^{3+},0.5%Ho^{3+} samples are compared under 980 and 1550 nm excitations with the same laser power. It is observed that the UCL intensities of the both samples under 1550 nm excitation is significantly higher than that excited by 980 nm laser. The integrated UCL intensity excited by 1550 nm is 11 and 10 times higher than that under 980 nm excitation for the $NaYS_2$:6%Er^{3+},1.5%Tm^{3+} and $NaYS_2$:6%Er^{3+},0.5%Ho^{3+} samples, respectively. This is due to the high efficiency absorbance at 1550 nm arising from the large absorption cross-section of the $^4I_{13/2}$ state of Er^{3+} ions. This is consistent with the results of reflectance spectra, i.e., the reflection peak at 1550 nm is much stronger than that at 980 nm as observed in Figure 2a.

The efficient red UCL is obtained after introducing Tm^{3+} or Ho^{3+} ions to $NaYS_2$:Er^{3+} phosphors. To investigate the impact of Tm^{3+} or Ho^{3+} ions on the UCL property of Er^{3+} self-sensitized $NaYS_2$, the UCL spectra and red to green emission intensity ratio (I_R/I_G) of $NaYS_2$:Er^{3+},Tm^{3+} and $NaYS_2$:Er^{3+},Ho^{3+} samples are shown in Figure 3. The $NaYS_2$:Er^{3+} sample without doping Tm^{3+} or Ho^{3+} exhibit a dominant green emission with a minor red emission. After the incorporation of Tm^{3+} or Ho^{3+} ions, the red UCL of the samples is significantly enhanced and gradually replaces the green UCL as the principal peak. The brightest red luminescence is achieved with a doping concentration of 1.5 mol%Tm^{3+} or 0.5 mol%Ho^{3+}. The insets of Figure 3a and c show the photo images of the phosphors under 1550 nm excitation. It can be observed that the color of the samples varies significantly from green to red after introducing the Tm^{3+} or Ho^{3+} ions. The I_R/I_G values increase from 0.17 to 4.73 and 4.90 with low concentration of Tm^{3+}% = 1.5 mol% and Ho^{3+}% = 0.5 mol%, respectively. The maximum I_R/I_G of $NaYS_2$:Er^{3+},Tm^{3+} and $NaYS_2$:Er^{3+},Ho^{3+} samples increase by 31 and 80 times compared to the $NaYS_2$:Er^{3+} sample, respectively (Figure 3b and d). These findings suggest that after doping Tm^{3+} or Ho^{3+} ions into $NaYS_2$:Er^{3+} sample, the luminescence color effectively changes from green to red.

Preprints (www.preprints.org) | NOT PEER-REVIEWED | Posted: 25 November 2023 doi:10.20944/preprints202311.1596.v1

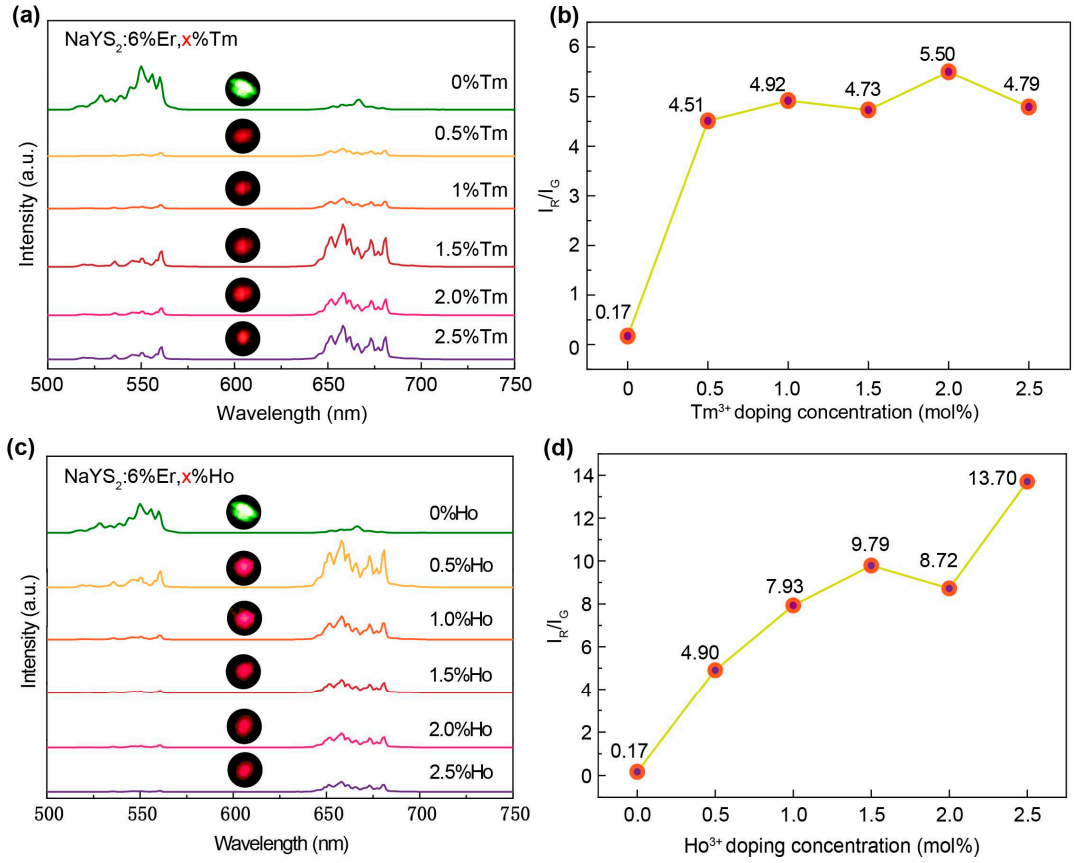

Figure 3. UCL spectra of (a) $NaYS_2$:6%Er^{3+},xTm^{3+} (x = 0, 0.5, 1.0, 1.5, 2.0, 2.5 mol%) and (c) $NaYS_2$:6%Er^{3+},xHo^{3+} (x = 0, 0.5, 1.0, 1.5, 2.0, 2.5 mol%) samples at 1550 nm excitation. The insets are the correspondence photo images of the phosphors. (b) and (d) are the I_R/I_G as a function of Tm^{3+}% and Ho^{3+}%, respectively.

To understand the UCL mechanism of samples, the fluorescence decay dynamics of $NaYS_2$:6%Er^{3+}, $NaYS_2$:6%Er^{3+},1.5%Tm^{3+} and $NaYS_2$:6%Er^{3+},0.5%Ho^{3+} samples were measured under 1550 nm excitation (Figures 4a, c and S1). According to the formula of

$$\tau = \frac{\int_0^\infty I(t)tdt}{\int_0^\infty I(t)dt} \quad (1)$$

where *I(t)* is the fluorescence luminescence intensity at time *t*. The calculated lifetime τ of the $^4S_{3/2}$ (555 nm), $^4F_{9/2}$ (655 nm) and $^4I_{9/2}$ (800 nm) levels are listed in Table 1. As shown in Figure 4b, the green-emitting state of $^4S_{3/2}/^2H_{11/2}(Er^{3+})$ is pumped through a simple continuous three-photon absorption processes from the ground state of $^4I_{15/2}$. Alternatively, the population of the red-emitting level of $^4F_{9/2}$ is more complicated. The critical step is to populate the $^4I_{11/2}$ state. Then after absorbing a 1550 nm photon, the Er^{3+} ions can be excited to the $^4F_{9/2}$ level for red UCL [23]. However, in the single-doped $NaYS_2$:Er^{3+} sample, the UCL spectra present highly dominant green with faint red emission at 1550 nm excitation (Figure 3a). This may due to the large energy gap between the $^4I_{9/2}$ and $^4I_{11/2}$ levels, making this multi-phonon relaxation (MPR) process ($^4I_{9/2} \rightarrow {}^4I_{11/2}$) difficult to occur [23]. When Tm^{3+} ions are incorporated, due to the characteristics of the energy structure of Tm^{3+} ions, the energy level of the $^4I_{9/2}(Er^{3+})$ matches with that of $^3H_4(Tm^{3+})$, resulting in energy transfer (ET) between Er^{3+} and Tm^{3+} ions, as indicated ET1 in Figure 4b. The Tm^{3+} ions act as an energy trapping center that effectively stored the transferred energy from Er^{3+} ions. This ET from Er^{3+} to Tm^{3+} ions can result in the lifetime (τ) shortening of the $^4I_{9/2}(Er^{3+})$ level, which is consistent with the τ measurements. As shown in Table 1, the τ of the $^4I_{9/2}$ level decrease significantly from 3432 μs ($NaYS_2$:Er^{3+}) down to 636 ($NaYS_2$:Er^{3+},Tm^{3+}). After that, the population of the $^4I_{11/2}$ level is achieved via cross-relaxation (CR) process of $^3H_4(Tm^{3+})$

Preprints (www.preprints.org) | NOT PEER-REVIEWED | Posted: 25 November 2023 doi:10.20944/preprints202311.1596.v1

+ $^4I_{13/2}(Er^{3+}) \rightarrow {}^3H_5(Tm^{3+}) + {}^4I_{11/2}(Er^{3+})$ (step 5 in Figure 4b). Then, the red-emitting state of $^4F_{9/2}$ are populated by further absorbing a 1550 nm photon or via energy transfer up-conversion (ETU) process of $^3F_4(Tm^{3+}) + {}^4I_{11/2}(Er^{3+}) \rightarrow {}^3H_6(Tm^{3+}) + {}^4F_{9/2}(Er^{3+})$ [6] (step 6 in Figure 4b). These energy transfer pathways after introducing Tm^{3+} ions effectively restrain the population of $^4I_{9/2}(Er^{3+})$ level, thereby achieving efficient red UCL.

Table 1. Fluoresce decay time of Er^{3+} $^4S_{3/2}$ (555 nm), $^4F_{9/2}$ (655 nm), $^4I_{9/2}$ (800 nm) levels in $NaYS_2$:6%Er^{3+}, $NaYS_2$:6%Er^{3+},1.5%Tm^{3+} and $NaYS_2$:6%Er^{3+},0.5%Ho^{3+} under 1550 nm excitation.

Energy levels (nm)	$NaYS_2:Er^{3+}$(μs)	$NaYS_2:Er^{3+},Tm^{3+}$ (μs)	$NaYS_2:Er^{3+},Ho^{3+}$ (μs)
555 ($^4S_{3/2}$)	2173	465	466
655 ($^4F_{9/2}$)	1346	481	347
800 ($^4I_{9/2}$)	3432	636	423

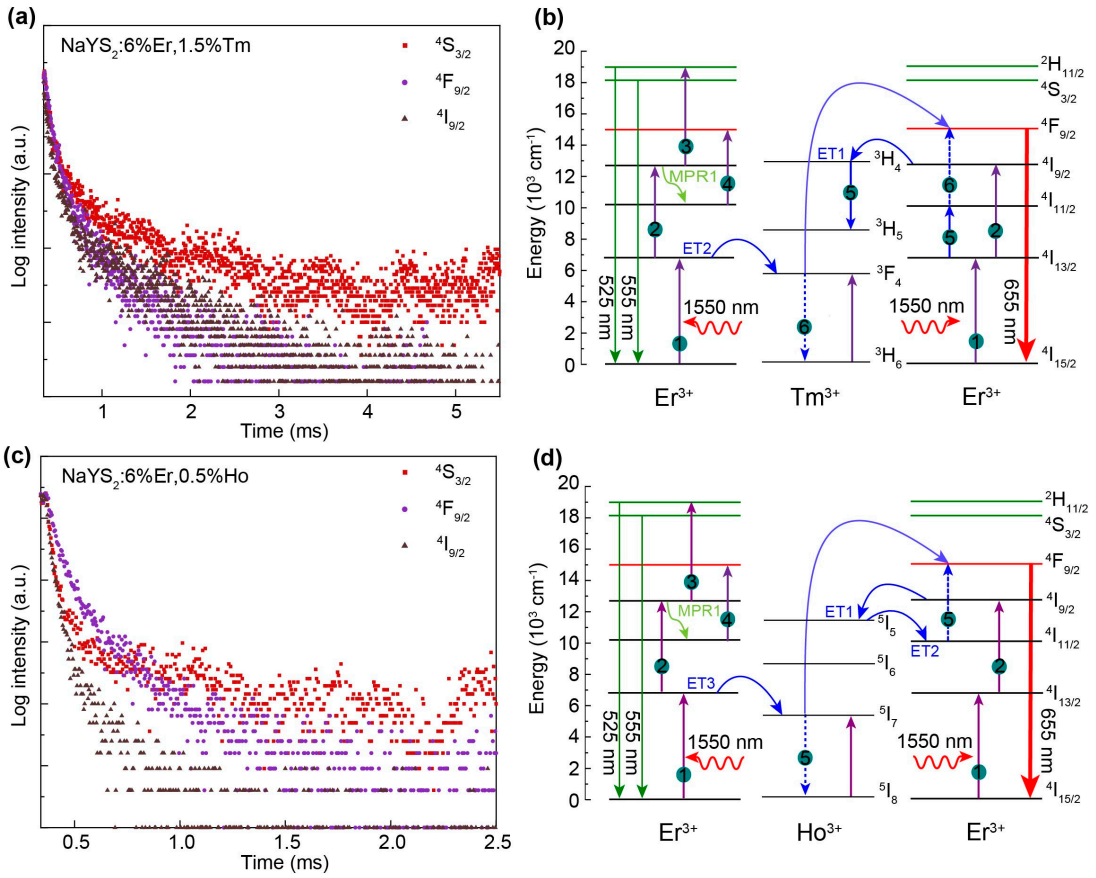

Figure 4. Fluoresce decay dynamics of $^4S_{3/2}$ (555 nm), $^4F_{9/2}$ (655 nm), $^4I_{9/2}$ (800 nm) energy levels of Er^{3+} ions in (a) $NaYS_2$:6%Er^{3+},1.5%Tm^{3+} and (c) $NaYS_2$:6%Er^{3+},0.5%Ho^{3+} under 1550 nm excitation. (b) and (d) are correspondence UCL mechanisms. ET and MPR represents energy transfer and multi-phonon relaxation processes, respectively.

When co-dope with Ho^{3+} ions, similar energy trapping process occurs in the $NaYS_2:Er^{3+},Ho^{3+}$ sample. As discussed above, the large energy gap between the $^4I_{9/2}$ and $^4I_{11/2}$ levels makes the MPR of $^4I_{9/2} \rightarrow {}^4I_{11/2}$ difficult to occur (MPR1). The energy state of $^5I_5(Ho^{3+})$ locates between $^4I_{9/2}$ and $^4I_{11/2}$ states and can store the energy transferred from the $^4I_{9/2}$ level of Er^{3+} via ET1, as illustrated in Figure 4d. Further, the $^4I_{11/2}$ state is populated via ET from Ho^{3+} to Er^{3+} ions (ET2). This ET processes are confirmed by the fluorescence decay dynamics which presents a reduction of the τ of $^4I_{9/2}(Er^{3+})$ level after doping the Ho^{3+} ions, i.e., the τ decreases from 3432 to 423 μs. After the population of the $^4I_{11/2}$ state, the red-emitting $^4F_{9/2}$ level are populated by further absorbing a 1550 nm photon or via ETU

Preprints (www.preprints.org) | NOT PEER-REVIEWED | Posted: 25 November 2023 doi:10.20944/preprints202311.1596.v1

process of $^5I_7(Ho^{3+}) + {}^4I_{11/2}(Er^{3+}) \rightarrow {}^5I_8(Ho^{3+}) + {}^4F_{9/2}(Er^{3+})$ (step 5 in Figure 4d). Therefore, the dominant red UCL is achieved in the $NaYS_2:Er^{3+},Ho^{3+}$ sample by altering the energy transfer pathways via Ho^{3+} ions.

3. Materials and Methods

The raw material used in this study were Y_2O_3 (99.99%), Er_2O_3 (99.99%), Tm_2O_3 (99.99%), Ho_2O_3 (99.99%), Na_2CO_3 (99.99%), and CS_2 (99.99%). The raw material was accurately weighed according to the chemical formula $NaY_{1-x-y}Er_xTm_yS_2$ (x = 6 mol%, y = 0.5, 1.0, 1.5, 2.0, 2.5 mol%) and $NaY_{1-x-y}Er_xHo_yS_2$ (x = 6 mol%, y = 0.5, 1.0, 1.5, 2.0, 2.5 mol%). The weighed powders were ground for 30 mins and placed into a corundum boat. Then samples were annealed at 1050 °C for 2 h in the atmosphere of argon and vapor of CS_2. After annealing, the $NaYS_2:Er^{3+},Tm^{3+}$ and $NaYS_2:Er^{3+},Ho^{3+}$ samples were cooled to room temperature under a flow of Ar.

X-ray diffraction (XRD) analysis was measured by using a SHIMADZU-6000 X-ray diffractometer (Cu-Kα radiation, λ = 0.15406 nm, 40 kV, 40 mA, 2θ = 10 ~ 80°). Scanning electron microscope (SEM) analysis was carried out with SUPRA 55 SAPPHIRE electron microscope. Diffuse reflectance spectra were measured with a UV-3600 Shimadzu UV-Vis-NIR spectrophotometer. Photoluminescence spectra and luminescence decay curves were recorded by using the Edinburgh FS5 spectrometer. Excitation sources were provided by a 1550 nm laser diode (CNI laser MDL-III-1550 nm) and a 980 nm laser diode (CNI laser MDL-III-980 nm) with tunable output power. The digital photos were taken using a Canon EOS 5D Mark III camera.

4. Conclusions

In summary, Er^{3+}/Tm^{3+} and Er^{3+}/Ho^{3+} co-doped $NaYS_2$ are prepared to realize red UCL under 1550 nm excitation. The $^4I_{9/2}(Er^{3+})$ level exhibits shorter lifetime after the addition of Tm^{3+} or Ho^{3+} ions due to the newly generated energy transfer pathways, which is beneficial for the population of $^4F_{9/2}$ level of Er^{3+} ions, realizing efficient red UCL. Therefore, the main emission peak is tuned from green to red successfully after the addition of Tm^{3+} or Ho^{3+} ions. The I_R/I_G of $NaYS_2:Er^{3+},Tm^{3+}$ and $NaYS_2:Er^{3+},Ho^{3+}$ samples increase by 31 and 80 times, respectively. The optimum doping concentration of Ho^{3+} and Tm^{3+} ions are 1.5 mol% and 0.5 mol%, respectively. The mechanisms of the red UCL and upconversion pathways are discussed in detail by steady-state fluorescence spectra and dynamics luminescence decay measurements. The findings demonstrate the achievement of red-emitting UCL within the ternary sulfide matrix, introducing a novel category of red UCL phosphors.

Supplementary Materials: The following supporting information can be downloaded at the website of this paper posted on Preprints.org, Figure S1: Fluoresce decay dynamics of $^4S_{3/2}$ (555 nm), $^4F_{9/2}$ (655 nm), $^4I_{9/2}$ (800 nm) energy levels of Er^{3+} ions in $NaYS_2$:6%Er^{3+}.

Author Contributions: Conceptualization, Y.T., X.L. and H.W.; methodology, J.W., L.W., K.C., Y.T. and H.W.; formal analysis, J.W., L.W., K.C. and H.W.; writing—original draft preparation, J.W. and K.C.; writing—review and editing, Y.T. and H.W.; supervision, Y.T. and X.L.; project administration, Y.T.; funding acquisition, Y.T and H.W. All authors have read and agreed to the published version of the manuscript.

Funding: This research was funded by the National Natural Science Foundation of China (Grant Nos. 12374404 and 12004063), the Fundamental Research Funds for the Central Universities (Grant No. 3132023193), and the Doctoral Start-up Foundation of Liaoning Province (Grant No. 2023-BS-076).

Institutional Review Board Statement: Not applicable.

Informed Consent Statement: Not applicable.

Data Availability Statement: Not applicable.

Conflicts of Interest: The authors declare no conflict of interest.

Preprints (www.preprints.org) | NOT PEER-REVIEWED | Posted: 25 November 2023 doi:10.20944/preprints202311.1596.v1

References

1. Li, C.X.; Lin, J. Rare Earth Fluoride Nano-/Microcrystals: Synthesis, Surface Modification and Application. *J. Mater. Chem.* **2010**, *20*, 6831-6847.
2. Gong, G.; Song, Y.; Tan, H.H.; Xie, S.W.; Zhang, C.F.; Xu, L.J.; Xu, J.X.; Zheng, J. Design of Core/Active-Shell $NaYF_4:Ln^{3+}@NaYF_4:Yb^{3+}$ Nanophosphors with Enhanced Red-Green-Blue Upconversion Luminescence for Anti-Counterfeiting Printing. *Compos. Pt. B-Eng.* **2019**, *179*, 107504.
3. Liu, Y.; Su, Q.Q.; Zou, X.M.; Chen, M.; Feng, W.; Shi, Y.B.; Li, F.Y. Near-Infrared in Vivo Bioimaging Using a Molecular Upconversion Probe. *Chem. Commun.* **2016**, *52*, 7466-7469.
4. Guan, Y.L.; Qu, S.N.; Li, B.; Zhang, L.M.; Ma, H.P.; Zhang, L.G. Ratiometric Fluorescent Nanosensors for Selective Detecting Cysteine with Upconversion Luminescence. *Biosens. Bioelectron.* **2016**, *77*, 124-130.
5. Liu, Y.W.; Yin, X.M.; Zhao, H.Z.; Shu, W.; Xin, F.Y.; Wang, H.; Luo, X.X.; Gong, N.; Xue, X.H.; Pang, Q.; Xing, M.M.; Tian, Y. Near-Infrared-Emitting Upconverting $BiVO_4$ Nanoprobes for in Vivo Fluorescent Imaging. *Spectroc. Acta Pt. A-Molec. Biomolec. Spectr.* **2022**, *270*, 120811.
6. Chan, E.M.; Han, G.; Goldberg, J.D.; Gargas, D.J.; Ostrowski, A.D.; Schuck, P.J.; Cohen, B.E.; Milliron, D.J. Combinatorial Discovery of Lanthanide-Doped Nanocrystals with Spectrally Pure Upconverted Emission. *Nano Lett.* **2012**, *12*, 3839-3845.
7. Wang, H.B.; Lu, W.; Yi, Z.G.; Rao, L.; Zeng, S.J.; Li, Z. Enhanced Upconversion Luminescence and Single-Band Red Emission of $NaErF_4$ Nanocrystals via Mn^{2+} Doping. *J. Alloy. Compd.* **2015**, *618*, 776-780.
8. Osseni, S.A.; Lechevallier, S.; Verelst, M.; Perriat, P.; Dexpert-Ghys, J.; Neumeyer, D.; Garcia, R.; Mayer, F.; Djanashvili, K.; Peters, J.A.; Magdeleine, E.; Gros-Dagnac, H.; Celsis, P.; Mauricot, R. Gadolinium Oxysulfide Nanoparticles as Multimodal Imaging Agents for T_2-Weighted MR, X-Ray Tomography and Photoluminescence. *Nanoscale* **2014**, *6*, 555-564.
9. Pei, Y.B.; Wei, M.Y.; Cheng, B.B.; Liu, Y.; Xie, Z.W.; Nguyen, K.; Yuan, B.H. High Resolution Imaging Beyond the Acoustic Diffraction Limit in Deep Tissue via Ultrasound-Switchable NIR Fluorescence. *Sci Rep* **2014**, *4*, 4690.
10. Zeng, S.J.; Yi, Z.G.; Lu, W.; Qian, C.; Wang, H.B.; Rao, L.; Zeng, T.M.; Liu, H.R.; Liu, H.J.; Fei, B.; Hao, J.H. Simultaneous Realization of Phase/Size Manipulation, Upconversion Luminescence Enhancement, and Blood Vessel Imaging in Multifunctional Nanoprobes through Transition Metal Mn^{2+} Doping. *Adv. Funct. Mater.* **2014**, *24*, 4051-4059.
11. Li, X.X.; Liu, L.; Fu, Y.; Chen, H.D.; Abualrejal, M.M.A.; Zhang, H.; Wang, Z.X.; Zhang, H.M. Peptide-Enhanced Tumor Accumulation of Upconversion Nanoparticles for Sensitive Upconversion Luminescence/Magnetic Resonance Dual-Mode Bioimaging of Colorectal Tumors. *Acta Biomater.* **2020**, *104*, 167-175.
12. Tian, G.; Gu, Z.J.; Zhou, L.J.; Yin, W.Y.; Liu, X.X.; Yan, L.; Jin, S.; Ren, W.L.; Xing, G.M.; Li, S.J.; Zhao, Y.L. Mn^{2+} Dopant-Controlled Synthesis of $NaYF_4$:Yb/Er Upconversion Nanoparticles for in Vivo Imaging and Drug Delivery. *Adv. Mater.* **2012**, *24*, 1226-1231.
13. Wang, F.; Liu, X.G. Recent Advances in the Chemistry of Lanthanide-Doped Upconversion Nanocrystals. *Chem. Soc. Rev.* **2009**, *38*, 976-989.
14. Hu, J.S.; Wang, R.N.; Wei, Z.Q.; Wu, X.; Wang, F.Y.; Liu, L.X.; Li, Y.Z.; Fu, H.; Xu, Q.H. Strong Red Upconversion Luminescence and Optical Thermometry of Yb^{3+}/Er^{3+} Co-Doped β-Ba_2ScAlO_5 Phosphor. *J. Alloy. Compd.* **2022**, *895*, 162692.
15. Xu, D.K.; Xie, F.Y.; Yao, L.; Li, Y.J.; Lin, H.; Li, A.M.; Yang, S.H.; Zhong, S.L.; Zhang, Y.L. Enhancing Upconversion Luminescence of Highly Doped Lanthanide Nanoparticles through Phase Transition Delay. *J. Alloy. Compd.* **2020**, *815*, 152622.
16. Berry, M.T.; May, P.S. Disputed Mechanism for NIR-to-Red Upconversion Luminescence in $NaYF_4:Yb^{3+},Er^{3+}$. *J. Phys. Chem. A* **2015**, *119*, 9805-9811.
17. Haase, M.; Schafer, H. Upconverting Nanoparticles. *Angew. Chem.-Int. Edit.* **2011**, *50*, 5808-5829.
18. Liu, L.; Wang, S.F.; Zhao, B.Z.; Pei, P.; Fan, Y.; Li, X.M.; Zhang, F. Er^{3+} Sensitized 1530 nm to 1180 nm Second Near-Infrared Window Upconversion Nanocrystals for in Vivo Biosensing. *Angew. Chem.-Int. Edit.* **2018**, *57*, 7518-7522.
19. Saha, S.; Pala, R.G.S.; Siyakumar, S. Catalyzing Cubic-to-Hexagonal Phase Transition in $NaYF_4$ via Ligand Enhanced Surface Ordering. *Cryst. Growth Des.* **2018**, *18*, 5080-5088.

Preprints (www.preprints.org) | NOT PEER-REVIEWED | Posted: 25 November 2023 doi:10.20944/preprints202311.1596.v1

20. Shang, Y.F.; Hao, S.W.; Lv, W.Q.; Chen, T.; Tian, L.; Lei, Z.T.; Yang, C.H. Confining Excitation Energy of Er^{3+}-Sensitized Upconversion Nanoparticles through Introducing Various Energy Trapping Centers. *J. Mater. Chem. C* **2018**, *6*, 3869-3875.
21. Yin, X.M.; Wang, H.; Tian, Y.; Xing, M.M.; Fu, Y.; Luo, X.X. Three Primary Color Emissions from Single Multilayered Nanocrystals. *Nanoscale* **2018**, *10*, 9673-9678.
22. Zhao, X.; Zhang, L.; Yan, X.; Zhang, L.; Lu, Y.; Pan, J.L.; Zhang, M.L.; Wang, C.G.; Suo, H.; Jia, X.T.; Liu, X.M.; Lu, G.Y. A Near-Infrared Light Triggered Fluormetric Biosensor for Sensitive Detection of Acetylcholinesterase Activity Based on $NaErF_4$:0.5%Ho^{3+}@$NaYF_4$ Upconversion Nano-Probe. *Talanta* **2021**, *235*, 122784.
23. Wang, H.; He, Z.; Cai, K.; Wei, L.M.; Xu, Y.; Fu, Y.; Xing, M.M.; Tian, Y. Designing Er^{3+} Single-Doped Ternary Sulfide for Highly Efficient Upconversion Luminescence under 1550 nm Excitation. *Chem. Eng. J.* **2023**, *468*, 143558.
24. Fábry, J.; Havlák, L.; Kuceráková, M.; Dusek, M. Redetermination of $NaGdS_2$, $NaLuS_2$ and $NaYS_2$. *Acta Crystallogr. Sect. C-Struct. Chem.* **2014**, *70*, 533-535.
25. Wu, H.; Hao, Z.D.; Zhang, L.L.; Zhang, X.; Xiao, Y.; Pan, G.H.; Wu, H.J.; Luo, Y.S.; Zhang, L.G.; Zhang, J.H. Er^{3+}/Yb^{3+} Codoped Phosphor $Ba_3Y_4O_9$ with Intense Red Upconversion Emission and Optical Temperature Sensing Behavior. *J. Mater. Chem. C* **2018**, *6*, 3459-3467.
26. Yin, X.M.; Xu, W.; Zhu, G.; Ji, Y.A.; Xiao, Q.; Dong, X.Y.; He, M.; Cao, B.S.; Zhou, N.; Luo, X.X.; Guo, L.; Bin, D. Towards Highly Efficient NIR II Response Up-Conversion Phosphor Enabled by Long Lifetimes of Er^{3+}. *Nat. Commun.* **2022**, *13*, 6549.
27. Brüesch, P.; Schüler, C. Raman and Infrared Spectra of Crystals with α-$NaFeO_2$ Structure. *J. Phys. Chem. Solids* **1971**, *32*, 1025-1038.
28. Jary, V.; Havlak, L.; Barta, J.; Buryi, M.; Mihokova, E.; Rejman, M.; Laguta, V.; Nikl, M. Optical, Structural and Paramagnetic Properties of Eu-Doped Ternary Sulfides $ALnS_2$ (A = Na, K, Rb; Ln = La, Gd, Lu, Y). *Materials* **2015**, *8*, 6978-6998.
29. Gerner, P.; Gudel, H.U. Absorption and Upconversion Light Emission Properties of Er^{3+} and Yb^{3+}/Er^{3+} Codoped $NaYS_2$. *Chem. Phys. Lett.* **2005**, *413*, 105-109.

Disclaimer/Publisher's Note: The statements, opinions and data contained in all publications are solely those of the individual author(s) and contributor(s) and not of MDPI and/or the editor(s). MDPI and/or the editor(s) disclaim responsibility for any injury to people or property resulting from any ideas, methods, instructions or products referred to in the content.